Eq. (4.5) at avarious elongation rates.

As mentioned before, two sets of experiments were conducted using two nozzles with different diameters. The obained volumetric flow rates versus applied external forces for fluids numbered 2, 3, and 4 are tabulated in Tables 2 and 3. By careful investigation of the results it can be deduced that the ratio of external forces are about equal to the ratio of volumetric flow rates for two diameters of nozzles. This important point can be of enormous usage for design and scale - up purposes.

Symbols

A (z)	cross - sectional area of the liquid colum
F	applied external force to the nozzle holder
g	gravitational acceleration
H	mean surface curvature
L	height of the liquid column taken as a characteristic length for the column
M	rate of momentum
n_r, n_z	vector components of the unit normal to the liquid column surface
p (r, z)	liquid pressure
Q	liquid volume flow rate
r	radial coorinate across the liquid column
R (z)	radius of the liquid column
R_0	radius of the column at the bottom of the liquid bead, i.e. at $z = z_0$
T	tensile force
v	velocity
W (z)	liquid weight in the column
W_0	liquid weight in the recirculation zone
z	axial coordinate along the liquid column

Greek symbols

$\dot{\gamma}$	rate- of-strain tensor, Eq. (2.5)
$\dot{\varepsilon}$ (z)	elongation rate, $\varepsilon = \partial v_z/\partial z$
$\bar{\eta}$ (z)	viscosity function
θ	angular coordinate
Π	total stress tensor, $\Pi_{ij} = p\,\delta_{ij} + \tau_{ij}$, where δ_{ij} is the Kronecker delta
ρ	fluid density
σ	surface tension of the fluid
τ	stress tensor

Supercript

'	prime symbole denotes differentiation with respect to z

References

[1] Denn, M. M., Process Modeling, Longman, New York (1986), Chap. 12, pp. 230-269.

[2] Denn, M. M. in J. R. A. Pearson and S. M. Richardson,eds., Computational Analysis of Polymer Processing, Applied Science, London (1983), Chap. 6. pp. 179-216.

[3] Pearson, J. R. A. Mechanics of Polymer Processing, Wiley, New York (1979).

[4] Peng, S. T. J. and Landel R. F. in Astarita, G., Marucci, G. and Nicolais, L. eds., Rheology, Vol 2, Plenum Press, New York (1980) pp. 385-391.

[5] Peng. S.T.J. and Landel, R.f.J. Apple. Phys., 47 (10) (1976) 4255.

[6] Astarita, G. and Nicodemo, L. Chem. Eng. J., 1 (1970) 57.

[7] Baid, K.M. and Metzner, A.B. Trans. Soc. Rheol., 21 (1977) 237.

[8] Fano, G. Archivio di Fisiologia, 5 (1908) 364.

[9] Astarita, G. and Nicodemo, L. Chem. Eng. J., 1 (1970) 57.

[10] Acierno, D., Titomanlio, G. and Nicodemo,L. Rheol. Acta, 15 (1974) 532.

[11] Bird, R. B. Armstrong. R. C. and Hassager, O. Dynamics of Polymeric Liquids, Vol. 1: Fluid Dynamics, John Wiley & Sons, New York 9 (1987).

[12] Balmer, R. T. J. Non-Newtonian Fluid Mech., 2 (1977) 307.

[13] Savarmand, S., Ph.D. Thesis, Amirkabir Univ. of Tech. (Tehran Polytechnic), Iran (1998)

[14] Kanel, F.A., Ph.D. Thesis, Univ. of Delaware, Newark (1972)

[15] Golcar N., M. R., Ph.D. Thesis, Bradford University (1978)

Table (1) Material Constants

Fluid No	1	2	3	4
σ (N/m)	0.060	0.06	0.060	0.060
ρ (kg/m^3)	1152	1160	1162	1173
η_0 (Nsm^{-2})	7.8	37.8	51.0	66.0
K (Ns^{n}m^{-2})	1.123	3.073	4311	6.368
n -	0.698	0.572	0.517	0.472

Table (2) Data for tubeless siphon nozzle 1 (D = 0.254 cm)

Fluid No	1	2	3	4
σ (N/m^2)	850.58	346.33	490.50	445.91
Q (mm^3)	555.6	824.7	402.0	208.3
α_0 (cm^{-n-1})	-20.4	-5.28	-.302	-12.09
b (cm^{-n})	207.7	95.4	3.31	77.7
m -	2.271	2.047	2.529	2.023
z_0 (cm)	0.1985	0.8169	0.3534	0.7223

Table (3) Data for tubeless siphon nozzle 2 (D = 0.356 cm)

Fluid No	1	2	3	4
σ (N/m^2)	850.58	1163.5	1224.6	543.82
Q (mm^3)	555.6	1269.8	921.4	279.7
α_0 (cm^{-n-1})	-20.4	-8.58	-24.26	-21.91
b (cm^{-n})	207.7	35.9	259.9	121.4
m -	2.271	2.950	2.996	2.870
z_0 (cm)	0.1985	0.2185	0.1175	0.5239

Conclusions

The method applied in this work may provide a suitable means to evaluate the variations of the elongational viscosity with respect to the elongation rate. It is worthwhile noting that normal stresses and therefore elongational viscosities shown in Figs. 9 and 10 are transient in nature because the velocity of a fluid element in the time dt changes as it moves to another point of the flow field where the velocity is different and therefore it gets some acceleration. With this emphasis, the results show that elongational viscosity has a very strong dependence on the elongation rate. Obtaining higher deformation rates may require to overcome the resulting higher shear viscosity that reduces the flow rate. To achieve higher elongation rate, the pressure difference between the nozzle entrance and the gradual cylinder would be increased to produce higher flow rates.

Furthermore, it can be seen from Figs. 9 and 10 that incresing the elongation rate causes increasing the elongational viscosity for solutions of PAA in glycerin/water mixtures of this work. This agrees with the results of Peng et al . [5]. In the present study, however, the existence of the liquid bead collected at the nozzle entrance, viz. the recirculation zone, and its effect on the analysis are considered while Peng et al. [5] ignored studying it through minimizing its formation by careful control of the liquid - column height that may not cancel its effect entirely.

A considerable feature of this analysis might be attributed to its capability of determining the contributions of all forces acting on the filament at various points along the column (Eqs. 3.24 to 27), and hence from

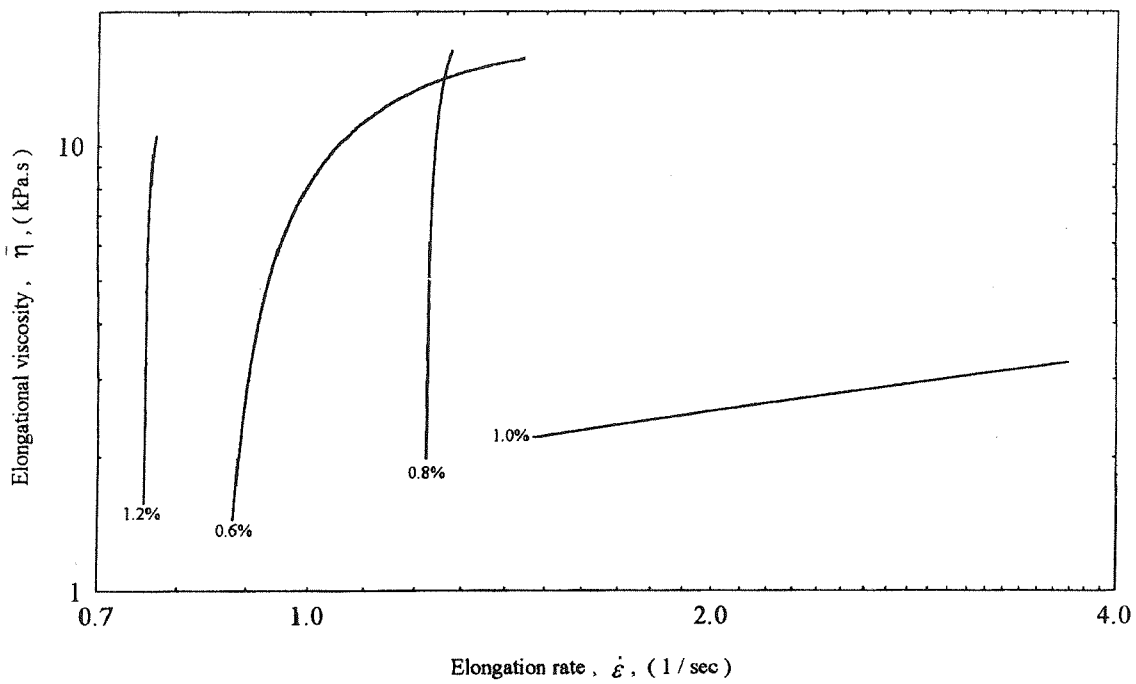

Fif (9) Elongational viscosity along the column vs. elongation rate for A: 0.6%, B: 0.8% C: 1.0% and D: 1.2% PAA in nozzle 1 (D = 0.254 cm)

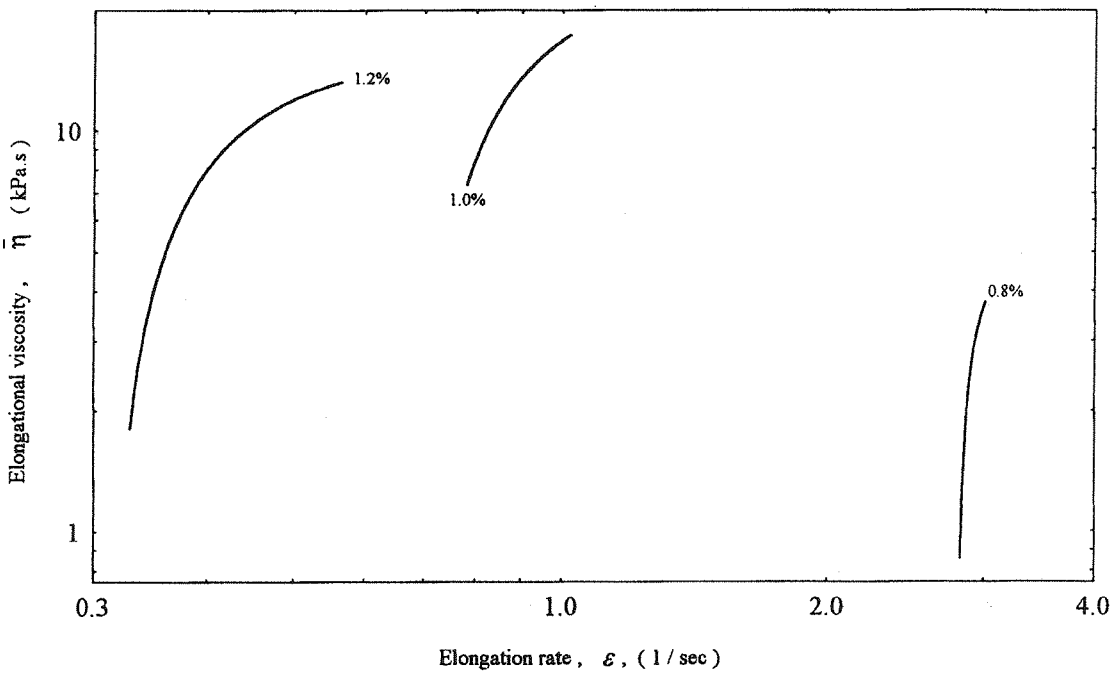

Fig (10) Elongational viscosity along the column vs. elongation rate for B: 0.8% C: 1.0% and D: 1.2% PAA in nozzle 2 (D = 0.356 cm)

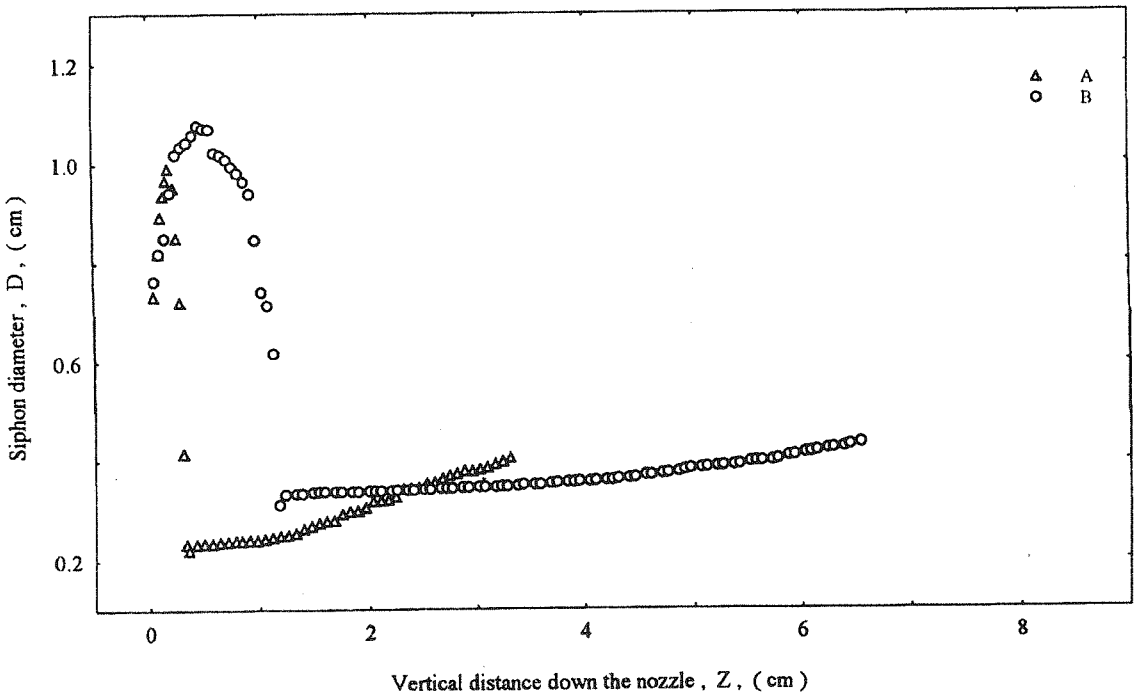

Fig (7) Siphn profile for solution of 1.0% AP-30 in a 50/50 mixture by wt. of glycerin / water in A: nozzle 1 (D = 0.254 cm), B: nozzle 2 (D = 0.356 cm)

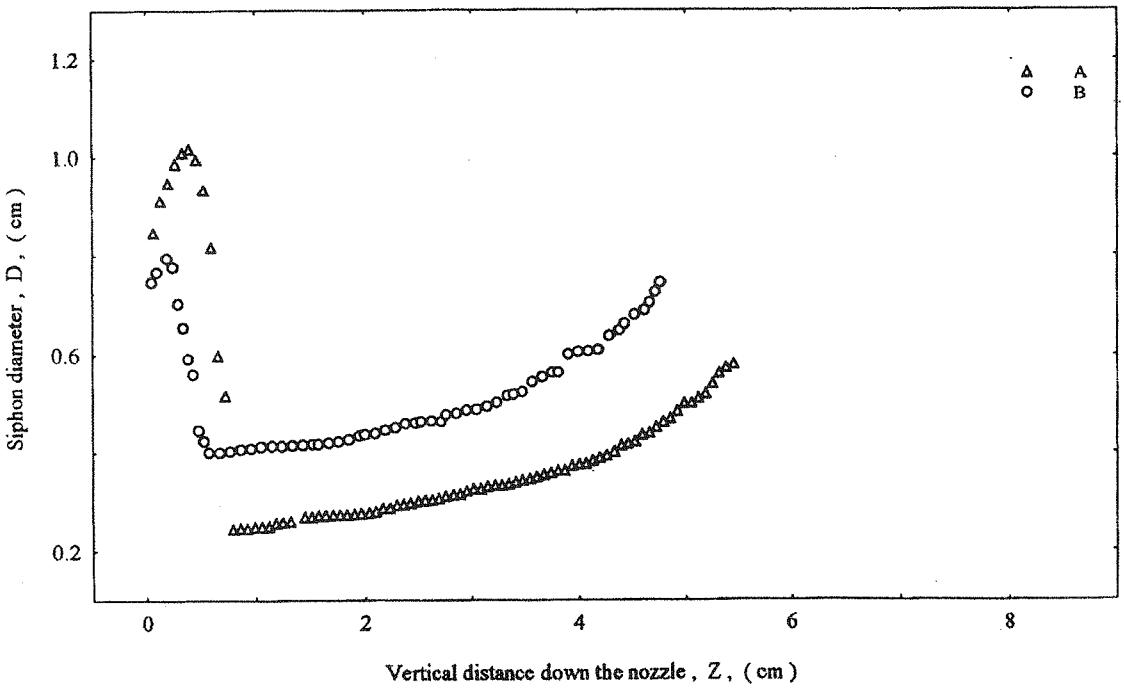

Fig (8) siphon profile for solution of 1.2% AP-30 in a 50/50 mixture by wt. of glycerin/water in A: nozzle 1 (D = 0.254 cm), B: nozzle 2 (D = 0.356cm)

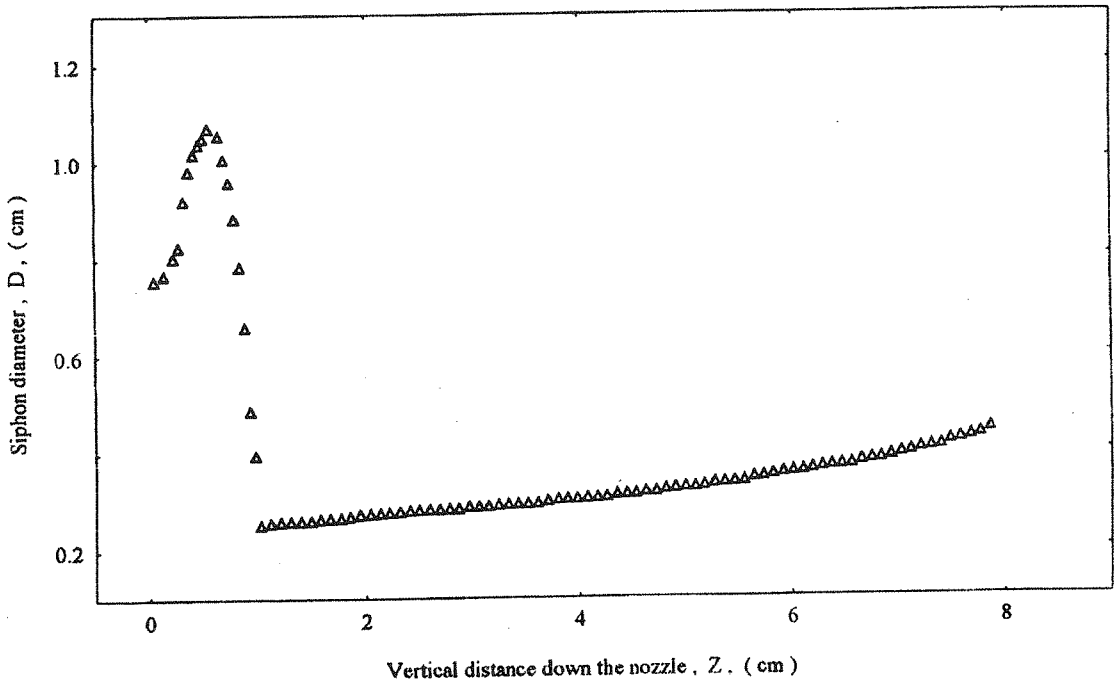

Fig (5) Siphon profile for solution of 0.6% AP - 30 in a 50/50 mixture by wt. of glycenrin / water in nozzle 1 (D = 0.254 cm)

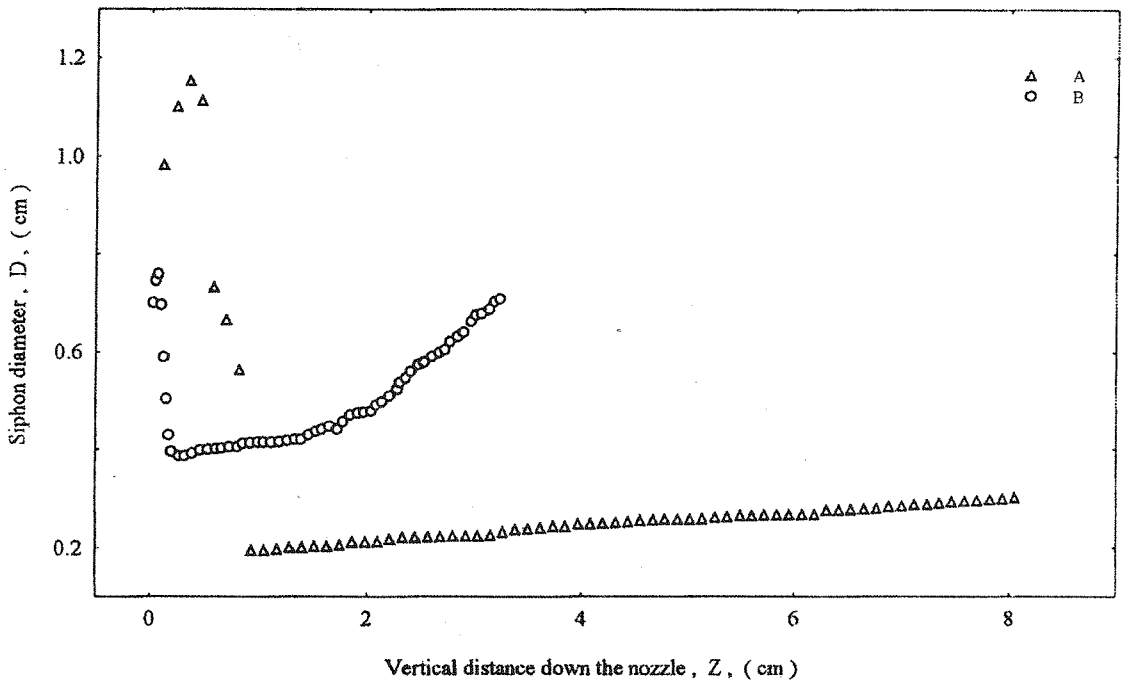

Fig (6) Siphon profile for solution of 0.8% AP - 30 in a 50/50 mixture by wt. of glycerin / water in A: nozzle 1 (D = 0.254 cm), B: nozzle 2 (D = 0.356cm)

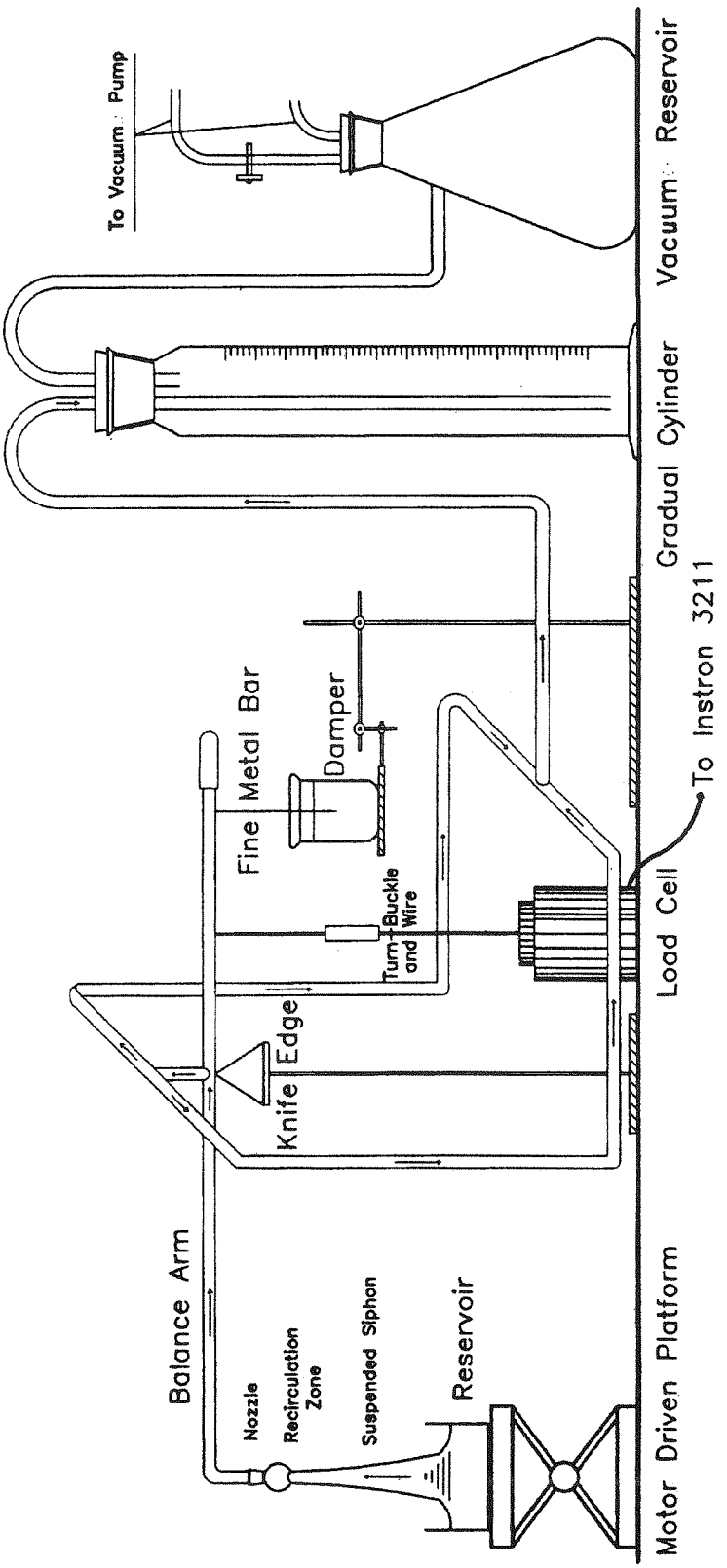

Fig (4) Schematic diagram of the tubeless - siphon apparatus

culation zone; second, the rest of the graph, i.e. the contraction region, that is the main column profile fitted by Eq. (4.1). The parameters of Eq. (4.1) are given in Tables 2 and 3. These tables also contain information about the applied external force F and the volume flow rate Q.

Using Eq. (5.1) and a knowledge of external force F (Tables 2 and 3), flow rate Q (Tables 2 and 3), and column profile R (z) (Section 4), the axial stress (Eq. 3.23), elongation rate (Eq. 4.2), and therefore the elongational viscosity (Eq. 5.1), may be obtained as functions of z. The results of elongational viscosities as functions of elongation rate for both nozzles are given in Figs. 9 and 10.

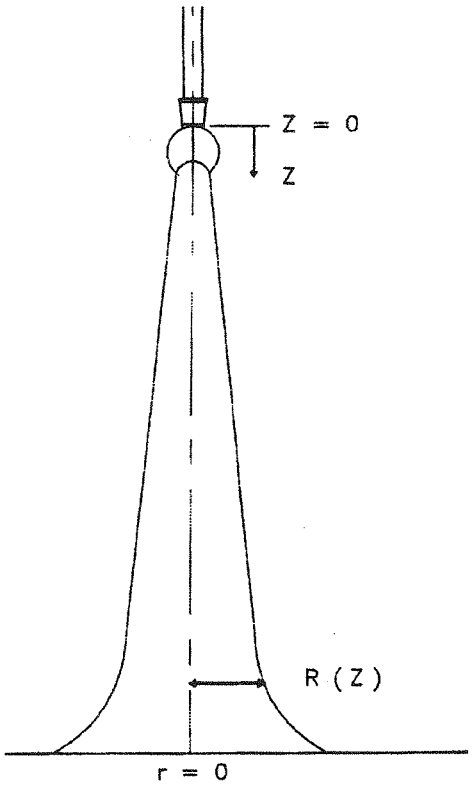

Fig (1) Schematic diagram of tubeless - siphon profile

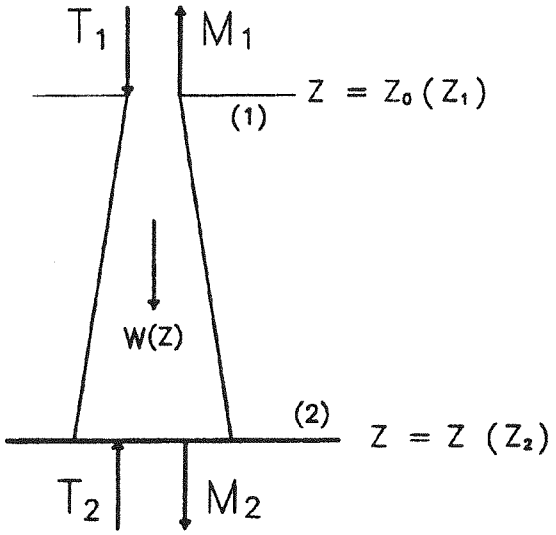

Fig (2) Free - body diagram for the right - angle bend of nozzle holder

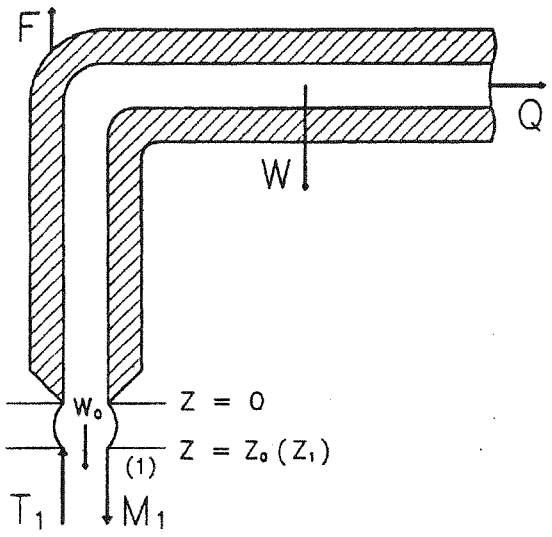

Fig (3) Free - body diagram for the suspended liquid filament

ninety-degree bend at one end and is pivoted on a knife edge.

The fluid leaves the balance arm through two exits opposite to each another. These exits are just above the knife edge and are perpendicular to the balance arm. This arrangement cancels any twisting motion caused by flowing fluid. The twisting torque is further reduced by having the two exits close to the knife edge.

Reducing any torque produced in the system is desirable. This is achieved by keeping the balance arm in a horizontal position (null position) using a turnbuckle and a wire, which connects the arm to the load cell.

After passing through the balance arm, the material is collected in a measuring cylinder, connected to a constant vacuum reservoir. This reservoir is a two-liter Buchner flask with bleeding facility consisting of a vertical outlet and a needle valve.

A Griffiths' rotary vacuum pump connected to the horizontal outlet of the Buchner flask is used to produce a vacuum in the system. The vacuum can be varied by either adjusting the needle valve on the Buchner falsk or the pump.

The force exerted by the liquid on the right - angle bend of the balance arm is measured by a load measuring system incorporated with an Instron type 3211 capillary rheometer. The load cell is an Instron type 2577 - 101 tensile load cell capable of measuring a maximum load of 500 grams. With this load - measuring system, tensile forces of 5, 10, 25, 50, 100, 250, and 500 grams (full scale readings) can be obtained.

A pen recorder is used to record the tensile force . The calibration of this recorder and measuring load system is discussed elsewhere [15].

6 - 3 - Experimental Procedure

The test liquid is first sucked up into the nozzle by allowing the tip of the nozzle to touch the free surface in the bath and connecting the nozzle to vacuum system simultaneously. The reservoir is then lowered gradually creating a column of liquid between the nozzle and the free surface. The rate of lowering the reservoir can be varied and is carefully controlled by means of a motor driven platform. By adjusting both the vacuum and rate of lowering the reservoir, a steady liquid column is stabilized; the reservoir is fixed and the flow rate is determined using a gradual cylinder.

The external force is then recorded by the pen recorder. Care has to be taken to carry out all the above measurements simultaneously. Photographs of the column are taken using an Exacta Camera, with combination of shutter speed and aperture. During photographing, different ASA films were used to obtain the sharpest picture of siphon outlines. For lighting the liquid column, a diffused light is obtained by placing a piece of opaque glass behind the reservoir and illuminating from the rear by a flashing lamp with a 50-watt bulb.

Results

In this study , in order to investigate the dependency of the liquid column on the nozzle diameter, two nozzles with diameters of 0.254 and 0.356 cm are used. The results of axial liquid column diameters for both nozzles are shown in Figs. 5 to 8. In the case of 0.6% PAA solution no continuous column was obtained with nozzle 2. These graphs consist of two parts: first, the short zone just down the nozzle entrance, i. e. the bulge region also called as the recir-

equation is the recirculation zone, $z \leq z_0$, consisting the bead of liquid collected at the nozzle entrance: to calculate W_0, the weight of the liquid bead, using the few measured data of $z \leq z_0$ with no curve - fitting procedure seems sufficient, Eq . (3. 14).

Note that Eq. (4.1) satisfies the homogeneous criterion, i.e. the constant stretch history for the flow field $v_i = \dot{\varepsilon}_{ij} x_j$. For example, for one - dimensional flow $v_1 = \dot{\varepsilon}_{11} x_1$ and from the continuity equation we obtain $1/R^2 = az$, for a homogeneous flow field. Thus, for Eq. (4.1) to hold the homogeneous criterion, m ought to be equal to 2. Then the value of m may convey some notion about the type of kinetics of the flow field: for $m > 2$ the elongation rate increases and for $m < 2$ decreases along z. From the continuity equation at each cross section of the siphon:

$$v_z = -\frac{Q}{A} = -Q/\pi R^2 \qquad (4.2)$$

thus

$$\frac{dv_z}{dz} = \dot{\varepsilon} = \frac{2Q}{\pi R^3}\frac{dR}{dz} \qquad (4.3)$$

Substitution of Eq. (4.1) into Eqs. (4. 2 and 3) yields:

$$v_z = -\frac{Q}{\pi}(az + b)^{2/m} \qquad (4.4)$$

$$\dot{\varepsilon} = -\frac{2aQ}{\pi m}(az + b)^{(2-m)/m} \qquad (4.5)$$

5 - Elongational Viscosity

The elongational viscosity may be defined as [11]:

$$\bar{\eta}(z) = \frac{(\tau_{zz} - \tau_{rr})|_z}{\dot{\varepsilon}(z)} \qquad (5.1)$$

6 - Experimental Work

6 - 1 - Rheological Measurement

Experimetal data were obtained on four solutions of different concentrations of polyacrylamide (Separan AP 30) in glycerin / water, Table 1. The solutions of 0.6%, 0.8%, 1.0% and 1.2% polyacrylamide in 50/50 mixtures by weight of glycerin / water are referred to as fluids no. 1, 2, 3 and 4 respectively.

Steady shear viscosity and normal forces with dynamic viscosity and storage modulus were measured using a Weissenberg rheogoniometer (model R - 18). For comparison, some parameters of the fluids in steady simple - shear flow, viz. zero-shear-rate viscosity η_0, parameters of power-law region K and n, are given in Table 1; extended data may be found elsewhere [15].

6 - 2 - Elongational Apparatus

The tubeless siphon is used for elongational flow measurements. A schematic view of the experimental apparatus used in this work is shown in Fig. 4. The sample to be elongated is placed in a rectangular prespex reservoir . The height on one side of the reservoir is three times bigger than that of the others. Photographs of the siphon were taken through this high prespex wall. This ensures that the entire siphon profile was observed under identical photographic conditions.

High frequency vibrations are reduced by means of a damper, which consists of a beaker full of high viscosity oil and a fine metal bar attached to the balance arm.

Elastic material is sucked upwards into the nozzle. The nozzle is connected to the vertical section of the balance arm. The balance arm is made of aluminum and has a

II - Momentum balance on the suspended liquid filament Fig. 3,

$$T_2 - T_1 - W(z) = M_1 - M_2 \qquad (3.17)$$

Where subscript 2 refers to the cross section (2),

$$M_2 = \int_0^{R_2} 2\pi r \rho v_z^2 (r, z_2)\, dr \qquad (3.18)$$

$$T_2 = \int_0^{R_2} 2\pi r\, \Pi_{zz} (r, z_2)\, dr \qquad (3.19)$$

$$W(z) = \rho g \int_{z_1}^{z_2} \pi R^2 (z)\, dz \qquad (3.20)$$

$$\Pi_{zz} (r, z_2) = p\ (r, z_2) + \tau_{zz} (r, z_2) \qquad (3.21)$$

Therefore , it can be shown that;

$$M_1 + T_1 = \int_0^{R_2} 2\pi r \left(\rho v_z^2 - \Pi_{zz}\right)_{(r, z_2)} dr$$

$$- \rho g \int_0^{z} \pi R^2(z)\, dz + \rho g \int_0^{z_0} \pi R^2(z)\, dz \qquad (3.22)$$

Eliminating $(M_1 + T_1)$ between Eqs. (3.16 and 22) and substituting the result into Eq. (3.10), knowing that $\tau_{rr} - \tau_{\theta\theta} = 0$ (see [11] pp 132), the following equation for the first normal stress is obtained (details are given by Savarmand [13]):

$$(\tau_{zz} - \tau_{rr})_{(z)} = \rho v_z^2 |_{(z)} + \frac{F}{\pi R^2 (z)} - \frac{\sigma}{R} (R(z) R''(z) - 1)$$

$$+ \frac{1}{\pi R^2 (z)} \int_{z_0}^{z} 2\pi\sigma R'(z) (R(z) R''(z) - 1)\, dz$$

$$- \frac{\rho g}{\pi R^2 (z)} \int_{z_0}^{z} \pi R^2 (z)\, dz - \frac{\rho g}{\pi R^2 (z)} \int_0^{z_0} \pi R^2 (z)\, dz \qquad (3.23)$$

From the above equation the following expressions can be made:

$$F_T = A(z)\, \Pi_{zz} (z) \qquad \text{(Tensile force)} \quad (3.24)$$

$$F_I = \rho A(z)\, V^2{}_z (z) \qquad \text{(Inertia force)} \quad (3.25)$$

$$F_G = \rho g \int_{z_0}^{z} \pi R^2 (z)\, dz + \rho g \int_0^{z_0} \pi R^2 (z)\, dz$$

(Gravity force) (3.26)

$$F_S = \sigma A(z) R''(z) - \pi R(z) \sigma - 2\pi\sigma \int_{z_0}^{z} R' \left(R (R'' - 1)\right) dz$$

(Surface force) (3 .27)

4 - Siphon Profile

The diameter of the siphon is mesured from enlarged photographs of the liquid column Fig. 1 , using a traveling microspace.

From a knowledge of the flow rate and R (z), the velocity gradient may be computed. Many attempts were made to fit the radius - distance data, with various types of curves; however, no satisfactory fit was found even with polynomial functions with more than 15 parameters. Therefore an empirical power law correlation [14] was used:

$$\frac{1}{R^m} = az + b \quad \text{or} \quad R = (az + b)^{-1/m} \qquad (4.1)$$

The above equation provides a satisfactory fit to the data of $z \geq z_0$ for all but a few points near the bottom of the column next to the liquid surface in the reservoir. Hence, the data are smoothed as far down from the bottom of the liquid bead at the nozzle entrance, i.e. $z = z_0$, as the equation can fit the profile with a curve - fitting error less than 1.5% . Another region not fitted by this

The prime symbol denotes differentiation with respect to z, n_r and n_z are the vector components of the unit normal to the surface, σ is the surface tension and H is the mean curvature.

Combining Eqs. (3.3) and (3.4), knowing that $\tau_{rz} = \tau_{zr}$, results in :

$$p(R, z) = p_0 - 2\sigma \frac{RR'' - R'^2 - 1}{2R(1 + R'^2)^{3/2}} + \frac{R'^2 \tau_{zz}(R, z)}{1 - R'^2} - \frac{\tau_{rr}(R, z)}{1 - R'^2} \quad (3.7)$$

$$\text{and } R'(\tau_{zz} - \tau_{rr})_{(R, z)} = -(1 - R'^2)\tau_{rz}(R, z) \quad (3.8)$$

Integrating Eq. (3 . 1) from r to R, assuming no contribution of shearing components, the pressure distribution can be obtained. Substituting p (R, z) from Eq. (3 . 7) into the latter and then substituting p (r, z) from the result into Eq. (3.1), leads to an equation for $\rho v_z (\partial v_z / \partial z)$. Further assuming $(dR/dz)^2 << 1$ and integrating the last equation from r = 0 to r = R (z), keeping z fixed, reads:

$$\int_0^R 2\pi r \rho v_z \frac{\partial v_z}{\partial z} dr = \frac{\partial}{\partial z}\int_0^R 4\pi r\sigma \frac{RR'' - 1}{2R} dr$$

$$-\frac{\partial}{\partial z}\int_0^R 2\pi \left[(\tau_{zz} - \tau_{rr})_{(r, z)} - \int_R^r (\tau_{\pi} - \tau_{\theta\theta\ (\xi, \tau)}\, d \ln\xi \right] dr + \pi R^2(z)\rho g \quad (3.9)$$

Integration of the above equation from $z = z_0$ (z_1) to z =z (z_2) yields:

$$\int_0^{R_2} 2\pi r \rho v_z^2(r, z_2)dr - \int_0^{R_1} 2\pi r \rho v_z^2(r, z_1)dr =$$

$$\left(\int_0^{R(z)} 4\pi r\, \sigma \frac{RR'' - 1}{2R} dr\right)_{Z_1}^{Z2} - \left\{\int_0^{R(z)} 2\pi r \left[(\tau_{zz} - \tau_{rr})_{(r, z)}\right.\right.$$

$$\left.\left. - \int_{R(z)}^{r} (\tau_{rr} - \tau_{\theta\theta})_{(\xi, z)}\, d \ln\xi \right] dr\right\}_{z_1}^{z_2} + \rho g \int_{z_1}^{z_2} \pi R^2(z)\, dz \quad (3.10)$$

Full details of derivations are given by Savarmand [13].

The working equation for the tensile stress can now be obtained using Eq. (3.10) and momentum balances on the right-angle bend of the nozzle holder and the suspended liquid filament:

(I) Applying the second law of motion to the right-angle bend of nozzle holder Fig. 2,

$$F + T_1 - W - W_0 = -M_1 \quad (3.11)$$

where subscript 1 refers to the cross section (1),

(Rate of momentum transferred by fluid)

$$M_1 = \int_0^{R(z_0)} 2\pi r \rho\, v_z^2(r, z_0)\, dr \quad (3.12)$$

(Tensile force)

$$T_1 = \int_0^{R(z_0)} 2\pi r\, \Pi_{zz}(r, z_0)\, dr \quad (3.13)$$

(Weight of liquid in the recirculation zone)

$$W_0 = \rho g \int_0^{z_0} \pi R^2(z)\, dz \quad (3.14)$$

F and W are the applied external force to the nozzle holder and the weight of liquid in the nozzle respectively and the total stress tensor is [11]:

$$\Pi_{zz}(r, z_0) = p(r, z_0) + \tau_{zz}(r, z_0) \quad (3.15)$$

It should be noted that the measuring system was calibrated to zero while full of liquid, therefore, W, may be dropped out from the momentum balance, thus

$$M_1 + T_1 = \int_0^{R(z_0)} 2\pi r \left(\rho v_z^2 - \Pi_{zz}\right)_{(r, z_0)} dr = -F + W_0 \quad (3.16)$$

$$v_1 = -\kappa\dot{\varepsilon}(1 + c)\, x_1 ;$$

$$v_2 = -\kappa\dot{\varepsilon}(1 - c)\, x_2 ;$$

$$v_3 = +\dot{\varepsilon}\, x_3 \qquad (2.1)$$

for cylindrical coordinates ($x_1 = r$, $x_2 = \theta$, $x_3 = z$), where $0 \le c \le 1$ and $\dot{\varepsilon}$ ($= \partial v_z / \partial z$) is the elongation rate [11] . When two elongation rates are equal, i. e. $c = 0$, and $\dot{\varepsilon} > 0$, then the motion is called an elongational flow. For incompressible materials. it is further required that $\nabla . v = 0$ that leads to $\kappa = 1/2$.

For steady axisymmetric flow, the continuity equation takes the form

$$\frac{1}{r}\frac{\partial}{\partial r}(r v_r) + \frac{\partial v_z}{\partial z} = 0 \qquad (2.2)$$

or

$$\frac{\partial}{\partial r}(r v_r) = -r\frac{\partial v_z}{\partial z} = -r\dot{\varepsilon} \qquad (2.3)$$

Integrating the above equation with the boundary condition $v_r = 0$ at $r = 0$, leads to

$$v_r = -\frac{r}{2}\dot{\varepsilon} \qquad (2.4)$$

Consequently the rate-of-deformation tensor is given by

$$\dot{\gamma} = \begin{pmatrix} -\dot{\varepsilon} & 0 & -\frac{r}{2}\frac{d\dot{\varepsilon}}{dz} \\ 0 & -\dot{\varepsilon} & 0 \\ -\frac{r}{2}\frac{d\dot{\varepsilon}}{dz} & 0 & 2\dot{\varepsilon} \end{pmatrix} \qquad (2.5)$$

The three diagonal terms in $\dot{\gamma}$ are all of the order $(Q / R_0^2 L^2)$, whereas the off-diagonal terms are of order $(Q / R_0^2 L^2)(R_0 / L)$. Since it is assumed that $R_0 / L << 1$, these terms will be neglected from now on; hence, flow in the column approximates an elongational in the sense that the largest components of the rate-of-strain tensor are the diagonal ones.

3 - Momentum Equations

The dynamics of an elongated filament shown in Fig. 1 is considered. In cylindrical coordinates, using assumptions made in the previous section, the following momentum balances can be written for steady axisymmetric flow field:

z - component

$$\rho\left(v_r\frac{\partial v_z}{\partial r} + v_z\frac{\partial v_z}{\partial z}\right) = -\frac{\partial p}{\partial z} - \frac{1}{r}\frac{\partial}{\partial r}(r\tau_{rz}) - \frac{\partial \tau_{zz}}{\partial z} + \rho g \qquad (3.1)$$

r - component

$$\rho\left(v_r\frac{\partial v_r}{\partial r} + v_z\frac{\partial v_r}{\partial z}\right) = -\frac{\partial p}{\partial r} - \frac{1}{r}\frac{\partial}{\partial r}(r\tau_{rr}) - \frac{\partial \tau_{rz}}{\partial z} + \frac{\tau_{\theta\theta}}{r} \qquad (3.2)$$

Considering the filament itself , at the free surface boundary of the siphon, the following boundary conditions apply:

$$2H\sigma n_r = \left[-p(R, z) - \tau_{rr}(R, z) + p_0\right] n_r - \tau_{rz}(R, z)\, n_z \qquad (3.3)$$

$$2H\sigma n_z = \left[-p(R, z) - \tau_{zz}(R, z) + p_0\right] n_z - \tau_{zr}(R, z)\, n_r \qquad (3.4)$$

$$v_r(R, z)\, n_r + v_z(R, z)\, n_z = 0 \qquad (3.5)$$

where

$$R = R(z) ; \qquad H = \left(RR'' - R'^2 - 1\right) / \left[2R\left(1 + R'^2\right)^{3/2}\right]$$

$$n_r = 1 / \left(1 + R'^2\right)^{1/2} ; \qquad n_z = -R' / \left(1 + R'^2\right)^{1/2} \qquad (3.6)$$

Since industrial flow processes are often elongational in character, steady shear data obtained in viscometers will be of little help in predicting flow behavior.

Many methods have been used to study elongational flows, such as fiber spinning and tubeless siphon, e. g. Denn [1 - 2] and Pearson [3] for fiber spinning; Peng and Landel [4 - 5], Astarita and Nicodemo [6] for tubeless siphon. Among these kinds of flows, spinning has been given more attention due to economical interests. In this process the material is subjected to a great amount of deformation within the die such that the stresses in the material are not zero when it reaches the elongation field as pointed out by Baid and Metzner [7]. The magnitude of these stresses depends on the deformation history of the material. In tubeless - siphon experiment, i. e. the main concern of this investigation, the material is in an underformed state in the reservoir before being extended.

The tubeless - siphon flow has been used to obtain elongational flow data for low - shear - viscosity polymer solutions. This type of flow was first addressed by Giulio Fano in 1908 [8]. In this flow, sometimes called as Fano flow, the material is drawn continuously into a nozzle connected to a vacuum pump. With viscoelastic fluids, a column of liquid will form and the flow continues by the tensile force associated with the elongational flow.

Astarita and Nicodemo [9] initiated research work on Fano flow. They discussed three types of theories, viz. exponential, complex phenomenological, and strength theories. Their observed data showed that simple forms of exponential theory correlates the data well and other two theories are not applicable.

Acierno et al. [10] carried out a theoretical and experimental approach to study the elongational flow of dilute polymer solutions. They used two techniques , viz. isothermal spinning and tubeless siphon, to obtain transient elongational viscosities from both processes. The observed elongational viscosities from both processes were found to increase with time where the velocity profiles were assumed to be linear. For tubeless siphon, however, this assumption is clearly not true for at least 1/4 of the data obtained by them. They failed to recognize that the tensile viscosity is a function of deformation rate [11].

Peng and Landel [5] pointed out that the elongational viscosity is a strong function of deformation rate and concentration of polymeric solutions. Their experimental results showed that the deformation rate varies along the liquid column.

The data of Balmer [12] in his investigations on the steady and unsteady simple elongational flows of Separan (Ap - 30) in glycerin / water using techniques similar to those of Astarita et al. [9], showed that inertia effects are not negligible and led to bulging and contraction of the liquid column. Balmer [12] used an average elongation rate and stated that the elongational viscosity increases with increasing elongation rate over the specified studied range. He also neglected the effects of surface forces that led to a considerable amount of error in elongational viscosity.

2 - Kinematics

Shear-free flows are given by the velocity field

Elongational Response of Viscoelastic Fluids in Tubeless-Siphon Experiment

S. Savarmand
Assistant Professor

M. R. Golcar Narenji
Associate Professor

S. M. Alaie
Assistant Professor

Faculty of Chemical Engineering Amirkabir Univesity of Technology

Abstract

The tubeless-siphon (Fano) flows of four solutions of polyacrylamide (PAA Dow Separan AP - 30), viz. 0.6, 0.8, 1.0, 1.2% in 50 / 50 mixtures by weight of glycerin and water are experimentally studied. A tubeless - siphon apparatus has been set up to evaluate elongational flow. The test fluid is sucked up into a nozzle by a vacuum system. A two dimensional momentum balance involving the free - surface geometry is applied with inertia effects included in the analysis. Free - body diagrams for the nozzle holder and the fluid are considered to relate the applied external force to the total stress tensor components; various forces could be applied and measured . The velocity profile may be obtained by means of photographing the fluid column and measuring the flow rate. To consider the effect of nozzle diameter, two nozzles are used. Data of liquid-column profile and computed elongational viscosity based on the analysis using experimental results are given graphically.

Keywords

Elongational flow; Viscoelastic fluids; Tubeless siphon; Elongational viscosity; Integral momentum balance.

Introduction

Various constitutive equations have been used to describe the rheological behavior of viscoelastic liquids; when the flow is elongational, there is a shortage of experimental data for comparative purposes. Therefore it is the objective of the present investigation to study quantitatively one such flow, viz. the tubeless -siphon experiment, and to provide rheological data for evaluating the performance of constitutive equations in future works.

Elongational flows are encountered in many industrial processes such as fiber spinning, film blowing, vacuum forming, blow molding, extrusion, and coating. Whenever in polymer processing, stream lines converge or diverge, an elongational deformation is present. In some of these processes, e. g. fiber spinning and film drawing, the dominant mode of deformation is one of elongation and not shear, however, in other cases, e.g. extrusion and injection molding, the material is subjected to fast changes in strain by either shear or elongation over a short time scale. Besides, there are processes in which a combination of both types of deformation may be encountered such as coating.